The Stability of Wave-like Pulsar Winds

Paul Withers, supervised by **Andrew Melatos** at the **California Institute of Technology**

Except where specific reference is made to the work of others, this work is original and has not been submitted either wholly or in part to satisfy any degree requirement at this or any other university.

Pulsars are heavy, compact, rapidly rotating stars, surrounded by intense electric and magnetic fields. Plasma near the pulsar surface is accelerated away from the pulsar by the fields to form a *pulsar wind*. The accepted, steady-state pulsar wind model does not correctly predict the observed energy transport in the wind. The wind contains both an electromagnetic and a kinetic energy component. Near the pulsar, the electromagnetic component is believed to dominate the energy flow. Steady-state wind theory predicts that the electromagnetic component will also dominate at large distances from the pulsar, where the wind slams into the surrounding nebula. However, observations show that the opposite is true. This inconsistency is known as the σ paradox.

Also, recent Hubble Space Telescope images have shown that the wind is not steady-state - the shock where the wind strikes the nebula has wisp-like structures varying on a time-scale of days.

A wave-like model has been proposed which solves this problem. This model is based on intense, relativistic plasma waves, which are potentially unstable: catastrophic energy loss due to radiation from the charges that make up the wind threatens to destroy the wave.

Using conservation of particles and energy, Maxwell's equations and a Lorentz force law I derive a set of five equations which must be satisfied by the wave-like wind in the limit of negligible radiation damping and certain other assumptions based on the nature of the pulsar wind. These show that the path of the particles in the wind is a helix.

Numerical and graphical approaches on Mathematica yielded a small number of solutions to these equations, and later analytic work gave a set of solutions throughout much of the wind region. In the region of greatest interest, close to the pulsar, the analytic work showed that the particle velocity along the direction of propagation is very close to the speed of light, yet the speed of rotation (and consequent acceleration) around the direction of propagation is very small. This suggests that the power radiated will be only a small fraction of the total energy in the wind.

The wind is re-energised each cycle as the pulsar rotates, so if it loses all its energy on a time-scale shorter than the pulsar period then the wave-like model is unstable. The ratio of energy in the wind to the rate at which it is radiated, or damping time, gives an estimate for this time-scale. Calculations of the damping time for all the solutions so far found predict that the wave-like model is extremely stable, with damping times many orders of magnitude greater than a single cycle.

Why are the intense relativistic plasma waves in a pulsar wind so stable, unlike cases studied previously? The main new feature in this model is *streaming*, the transport of particles away from the pulsar. Analytic work on the forces acting on the particles in the wind suggest that this is of crucial importance.

1 - Pulsars and their Outflows

The tendency for a star to collapse under gravity is resisted during its lifetime by the burning of hydrogen and helium. When the fuel supply is exhausted, the outer layers of the star are ejected in a supernova and the core is compressed by gravitational collapse. The core has a final diameter of about 20km and is as dense as an atomic nucleus. The explosion releases as much energy as is radiated by a galaxy of 10 billion stars in a week. The core, which is called a *pulsar*, is also highly energetic.

Before the explosion, the core was rotating slowly. Conservation of angular momentum causes the pulsar to rotate rapidly, up to a few hundred times per second. The dipolar magnetic field around the star is increased in strength during the explosion, to conserve magnetic flux. Like a dynamo, the pulsar generates intense electric fields as well. (Shapiro and Teukolsky, 1983)

The most well-known aspect of pulsars is their regularly pulsing radio beacon. A beam of radio waves is emitted along the magnetic axis. If this axis is different to the rotation axis, then distant observers see a series of pulses. These pulses are very regular, with a period equal to the rotational period of the pulsar. This period is universally observed to decrease with time, at a rate on the order of 10^{-5} s s^{-1}. By considering the loss of rotational kinetic energy, we find that the pulsar is losing many times more energy than can be explained by the radio emissions.

The intense electromagnetic fields create electrons and positrons close to the pulsar surface. This *plasma* is accelerated away from the pulsar by the same fields, forming an ultra-relativistic outflow. This *pulsar wind* is the primary way in which pulsars lose energy.

1.1 - The Pulsar Wind

Traditionally, the pulsar wind is considered, like the solar wind, to be a steady-state wind; that is, its properties at any point do not change with time. This model has a number of problems:

a) The wind contains both an electromagnetic and a kinetic energy component. Near the pulsar, the electromagnetic component is believed to dominate the energy flow. Steady-state wind theory predicts that the electromagnetic component will also dominate at large distances from the pulsar, where the wind slams into the surrounding nebula. However, observations have shown that the opposite is true - kinetic energy must dominate at this boundary in order for the expansion speed and pressure at the edge of the nebula to match the values observed (Kennel & Coroniti, 1984). This inconsistency is known as the σ paradox.

b) Recent Hubble Space Telescope images have shown that the wind is not steady-state (Hester et al, 1995; www.stsci.edu) - the shock where the wind strikes the nebula contains wisp-like structures which vary on a time-scale of days.

c) Many scientists have long held that a giant rotating electromagnet should cause the pulsar wind to oscillate at the rotation frequency in some way.

In my opinion, the steady-state model has only been accepted in light of these criticisms because the alternative model has a few problems of its own, which were previously thought to render it useless. The alternative model is that the wind is wave-like. It is important to emphasis and understand the strength of this wave. It is not a mere ripple disturbing the charges; it is more like a giant tidal wave hurling the charges around with immense force. It is strong enough to accelerate the charges to ultra-relativistic speeds.

My supervisor for this vacation project has proposed (Melatos & Melrose, 1996) a wave-like model which correctly predicts the oscillating nature of the wind and resolves the σ paradox.

1.2 - The Stability of Wave-Like Pulsar Winds

The problem with most wave-like models is their stability. Unlike a steady-state wind, a wave-like wind loses energy because the charges that make up the wind are accelerated by the electromagnetic fields and radiate. The wave is re-energised each cycle as the pulsar rotates, so if the wind loses all its energy on a timescale shorter than the pulsar period then the wave-like model is unstable.

Previous work (Asseo et al, 1978) has shown that intense relativistic plasma waves are heavily damped by radiation in certain circumstances. The aim of this vacation project was to investigate radiative damping in the context of pulsar winds.

The wave can also be destroyed by the amplification of perturbations (Max & Perkins, 1972; Sweeney & Stewart, 1978) due to hydromagnetic instabilities. This was investigated by Ronak Bhatt, a Caltech student performing a vacation project with the same supervisor as myself. His preliminary results suggest that the wave is stable against this type of instability.

1.3 - Work Performed on Vacation Project

The main aim of the project was to obtain *damping times* for the wave-like model. The damping time is the ratio of energy in the wind to the rate at which energy is lost by the wind. If the damping time is shorter than one cycle then the wave-like model is not viable.

My actual work fell into three categories:

a) Analytical work to obtain useful algebraic and differential equations, find limiting cases of these.

b) Use Mathematica to numerically and graphically solve equations, evaluate errors and display results.

c) Write Fortran code to integrate the differential equations I obtained.

2 - Modelling the Pulsar Wind

The pulsar wind is modelled as an e^+e^- plasma, in which the electrons and positrons individually behave like cold fluids and are completely characterised by lab-frame number densities $n^\pm$ and lab-frame velocities $\mathbf{v}^\pm$. Here, and henceforth, superscripts - and + refer to electrons and positrons respectively. Each fluid obeys a particle conservation law

$$\frac{\partial n^\pm}{\partial t} + \nabla.(n^\pm \mathbf{v}^\pm) = 0\,. \tag{1}$$

Each fluid obeys a Lorentz equation of motion

$$\frac{\partial \mathbf{p}^\pm}{\partial t} + (\mathbf{v}^\pm.\nabla)\mathbf{p}^\pm = \pm e(\mathbf{E} + \mathbf{v}^\pm \times \mathbf{B}) + \mathbf{RR}^\pm\,, \tag{2}$$

$$\mathbf{RR}^\pm = \frac{e^2}{6\pi\varepsilon_0 c^3}\left\{\gamma^\pm \frac{d}{dt}\left[\gamma^\pm \frac{d}{dt}(\gamma^\pm \mathbf{v}^\pm)\right] - \frac{\gamma^{\pm 4}}{c^2}\left[\frac{\gamma^{\pm 2}}{c^2}\left(\mathbf{v}^\pm.\frac{d\mathbf{v}^\pm}{dt}\right)^2 - \left(\frac{d\mathbf{v}^\pm}{dt}\right)^2\right]\right\}\gamma^\pm \mathbf{v}^\pm\,, \tag{3}$$

where $\mathbf{p}^\pm = \gamma^\pm m\mathbf{v}^\pm$ is the relativistic 3-momentum of each fluid, $\gamma^\pm$ is the associated Lorentz factor and $\mathbf{RR}^\pm$ is the Radiation Reaction force; the rate at which momentum is carried away by the radiation field of a radiating charge. If the wave-like model is stable against radiation losses then $\mathbf{RR}^\pm$ will be negligible.

The electromagnetic fields $\mathbf{E}$ and $\mathbf{B}$ in (2) are self-consistent fields generated by the charge and current densities in the plasma, and satisfy Maxwell's equations with two-fluid source terms:

$$\nabla.\mathbf{E} = \frac{e}{\varepsilon_0}\left(n^+ - n^-\right), \tag{4}$$

$$\nabla.\mathbf{B} = 0, \tag{5}$$

$$\nabla \times \mathbf{E} = -\frac{\partial \mathbf{B}}{\partial t}, \tag{6}$$

$$\nabla \times \mathbf{B} = \mu_0 e\left(n^+ - n^-\right) + \frac{1}{c^2}\frac{\partial \mathbf{E}}{\partial t}, \tag{7}$$

We look for travelling wave solutions depending on $\mathbf{x}$ and t through the phase

$$\chi = \omega t - \mathbf{k}.\mathbf{x} = \omega\left(t - \frac{\boldsymbol{\kappa}.\mathbf{x}}{\beta c}\right), \tag{8}$$

where $\beta = \dfrac{\omega}{c|\mathbf{k}|}$ is the reciprocal of the refractive index and $|\boldsymbol{\kappa}| = 1$.

Thus, $\nabla \rightarrow -\left(\dfrac{\omega\boldsymbol{\kappa}}{\beta c}\right)\dfrac{d}{d\chi}$ and $\dfrac{\partial}{\partial t} \rightarrow \omega\dfrac{d}{d\chi}$ (9) , (10)

(This section adapted from Melatos and Melrose, 1996)

2.1 - Equations of Motion for the Pulsar Wind

Before my arrival, my supervisor had made some assumptions and proceeded to derive equations of motion from these equations. He neglected $\mathbf{RR}^{\pm}$ and assumed that there was no uniform, static component of $\mathbf{B}$. Neglecting $\mathbf{RR}^{\pm}$ means that the wave is *undamped*. The uniform, static component of $\mathbf{B}$ is a constant of integration in the derivation.

He found that $n^{\pm} = \dfrac{n_0}{1 - \dfrac{\boldsymbol{\kappa}.\mathbf{v}^{\pm}}{\beta c}}$, (11)

where the boundary condition $n^{\pm} = n_0$ when $\mathbf{v}^{\pm} = 0$ was used, and defined

$$\omega_0^2 = \frac{n_0 e^2}{m\varepsilon_0}. \tag{12}$$

This gives the following equations of motion for a wave propagating in the z direction:

$$\frac{d^2\rho_x^{\pm}}{d\chi^2} \pm \frac{\omega_0^2\beta^3}{\omega^2\left(\beta^2 - 1\right)}\left(\frac{\rho_x^+}{\beta\gamma^+ - \rho_z^+} - \frac{\rho_x^-}{\beta\gamma^- - \rho_z^-}\right) = 0 \ , \tag{13}$$

$$\frac{d^2\rho_y^{\pm}}{d\chi^2} \pm \frac{\omega_0^2\beta^3}{\omega^2\left(\beta^2 - 1\right)}\left(\frac{\rho_y^+}{\beta\gamma^+ - \rho_z^+} - \frac{\rho_y^-}{\beta\gamma^- - \rho_z^-}\right) = 0 \ , \tag{14}$$

$$\frac{d^2}{d\chi^2}\left(\beta\rho_z^{\pm} - \gamma^{\pm}\right) \pm \frac{\omega_0^2\beta^3}{\omega^2}\left(\frac{\gamma^+}{\beta\gamma^+ - \rho_z^+} - \frac{\gamma^-}{\beta\gamma^- - \rho_z^-}\right) = 0 \ , \tag{15}$$

where $\rho^{\pm}$ is the dimensionless momentum given by $\rho^{\pm} = \dfrac{\mathbf{p}^{\pm}}{mc} = \dfrac{\gamma^{\pm}\mathbf{v}^{\pm}}{c}$. We considered plane waves exclusively during this vacation project. My supervisor's derivation of (13) - (15) can be seen in appendix A.

Physically, the assumption of no uniform, static component of $\mathbf{B}$ is an oversimplification. I derived the following generalisation of (13) - (15):

$$\frac{d^2\rho_x^{\pm}}{d\chi^2} \pm \frac{\omega_0^2\beta^3}{\omega^2\left(\beta^2-1\right)}\left(\frac{\rho_x^+}{\beta\gamma^+ - \rho_z^+} - \frac{\rho_x^-}{\beta\gamma^- - \rho_z^-}\right)$$
$$\mp \frac{e\beta}{m\omega}\left(\frac{B_{0z}}{\beta c}\frac{d}{d\chi}\left(\frac{v_y^{\pm}}{1-\frac{v_z^{\pm}}{\beta c}}\right) - B_{0y}\frac{d}{d\chi}\left(\frac{1}{1-\frac{v_z^{\pm}}{\beta c}}\right)\right) = 0 \quad , \tag{16}$$

$$\frac{d^2\rho_y^{\pm}}{d\chi^2} \pm \frac{\omega_0^2\beta^3}{\omega^2\left(\beta^2-1\right)}\left(\frac{\rho_y^+}{\beta\gamma^+ - \rho_z^+} - \frac{\rho_y^-}{\beta\gamma^- - \rho_z^-}\right)$$
$$\pm \frac{e\beta}{m\omega}\left(\frac{B_{0z}}{\beta c}\frac{d}{d\chi}\left(\frac{v_x^{\pm}}{1-\frac{v_z^{\pm}}{\beta c}}\right) - B_{0x}\frac{d}{d\chi}\left(\frac{1}{1-\frac{v_z^{\pm}}{\beta c}}\right)\right) = 0 \quad , \tag{17}$$

$$\frac{d^2}{d\chi^2}\left(\beta\rho_z^{\pm} - \gamma^{\pm}\right) \pm \frac{\omega_0^2\beta^3}{\omega^2}\left(\frac{\gamma^+}{\beta\gamma^+ - \rho_z^+} - \frac{\gamma^-}{\beta\gamma^- - \rho_z^-}\right)$$
$$\pm \frac{e\beta}{m\omega c}\frac{d}{d\chi}\left(\frac{B_{0x}v_y^{\pm} - B_{0y}v_x^{\pm}}{1-\frac{v_z^{\pm}}{\beta c}}\right) = 0 \quad , \tag{18}$$

These, of course, reduce to (13) - (15) when $\mathbf{B}_0$, the uniform, static $\mathbf{B}$, is set equal to zero. My derivation of this can be seen in appendix B.

2.2 - Solution of the Equations of Motion

To solve these equations it was necessary to make some more assumptions, guided by the physical nature of the pulsar wind. We assumed that:

$$\mathbf{B}_0 = B_0\boldsymbol{\kappa} \ , \tag{19}$$

$$\boldsymbol{\kappa}.\mathbf{E} = 0 \ , \tag{20}$$

$$\boldsymbol{\kappa}.\rho^{\pm} = \text{constant} \tag{21}$$

$\mathbf{E}$ is circularly polarised, i.e. $E_x \sim \sin\chi, E_y \sim \cos\chi$ (22)

Equation (20) and page 2 of appendix A imply that $n^+ = n^-$, (23)

and hence (11) implies that $\boldsymbol{\kappa}.\mathbf{v}^+ = \boldsymbol{\kappa}.\mathbf{v}^-$. (24)

ρ_z^+ and ρ_z^- are constant, but if they are equal then electrons and positrons behave identically. This is unphysical, as the magnetic field differentiates between them. Thus, ρ_z^+ and ρ_z^- are not equal. We can also state that γ^+ and γ^- are constant but not equal. Appendix C derives the following solution.

Polarisation State	E_x	E_y	ρ_x^+	ρ_y^+	ρ_x^-	ρ_y^-
A	$E_0\cos\chi$	$-E_0\sin\chi$	$\rho_\perp^+ \sin\chi$	$\rho_\perp^+\cos\chi$	$-\rho_\perp^- \sin\chi$	$-\rho_\perp^- \cos\chi$
	$E_0 > 0$		$\rho_\perp^+ >< 0$		$\rho_\perp^- > 0$	
B	$E_0\cos\chi$	$E_0\sin\chi$	$\rho_\perp^+\sin\chi$	$-\rho_\perp^+\cos\chi$	$-\rho_\perp^-\sin\chi$	$\rho_\perp^-\cos\chi$
	$E_0 > 0$		$\rho_\perp^+ > 0$		$\rho_\perp^- >< 0$	

The path of the particles is a helix, with the speeds along the axis greatly exceeding their speeds of rotation about the axis (shown in section 4.1, (45)). The presence of a background magnetic field causes the electrons and positrons to rotate at different speeds; those rotating in the same sense as their gyration rotate fastest.

The sign ambiguities above mean that equations (25) must be squared before they can be used.

The two polarisation states obey the following equations:

State A $$\upsilon_0 = \rho_\perp^{\pm}\left(1 \mp \frac{\Omega_0}{w\gamma^{\pm}}\frac{1}{1-\frac{v_z^{\pm}}{\beta c}}\right)$$

State B $$\upsilon_0 = \rho_\perp^{\pm}\left(1 \pm \frac{\Omega_0}{\omega\gamma^{\pm}}\frac{1}{1-\frac{v_z^{\pm}}{\beta c}}\right) \tag{25}$$

where $\upsilon_0 = \dfrac{eE_0}{mwc}$ and $\Omega_0 = \dfrac{eB_0}{mc}$ (26) , (27)

The two polarisation states may be switched by reversing the sign of Ω_0.

Both polarisation states obey the following dispersion relation

$$\frac{\omega^2}{\omega_0^2}\left(1-\frac{1}{\beta^2}\right)=\frac{1}{\gamma^+(1-\frac{v_z^+}{\beta c})+\frac{\Omega_0}{\omega}}+\frac{1}{\gamma^-(1-\frac{v_z^-}{\beta c})-\frac{\Omega_0}{\omega}} \qquad (28)$$

Phase-averaged conservation of particle number and energy yield two more equations, derived in appendix D.

$$\frac{\omega_0^2}{\omega^2}=\frac{Ne^2}{8\pi\varepsilon_0 mc^3}\frac{1-\frac{v_z^\pm}{\beta c}}{\frac{v_z^\pm}{c}}\left(\frac{r}{r_L}\right)^{-2}, \qquad (29)$$

$$\frac{\omega^2\upsilon_0^2}{\omega_0^2\beta}+\frac{\left(\gamma^++\gamma^-\right)\frac{v_z^\pm}{c}}{1-\frac{v_z^\pm}{\beta c}}=\frac{Le^2}{4\pi\varepsilon_0 m^2c^5}\frac{\omega^2}{\omega_0^2}\left(\frac{r}{r_L}\right)^{-2}, \qquad (30)$$

where N is the number of particles injected into the wind by the pulsar per second, L is the power fed into the wind by the pulsar and r_L is the light cylinder radius, a characteristic distance equal to $\frac{c}{\omega}$.

2.3 - Initial Numerical Results

We can use observational data to obtain L, N and ω. Our unknowns are $\beta, \frac{\omega_0}{\omega}, \upsilon_0, \rho_\perp^+, \rho_\perp^-, \frac{\Omega_0}{\omega}$ and $\frac{v_z^\pm}{c}$. It seems most reasonable to stipulate that the latter two unknowns are functions of r, $\frac{v_z^\pm}{c}$ being independent of r and $\frac{\Omega_0}{\omega}\propto r^{-2}$.

Both $\frac{v_z^\pm}{c}$ and β are only slightly less than unity. The numerical problems this causes can easily be envisaged by reference to the previous section. To ease mental anguish when dealing with these two variables, replacement variables were introduced:

$$\delta=1-\beta, \qquad (31)$$

$$\Gamma=\left(1-\left(\frac{v_z^\pm}{c}\right)^2\right)^{\frac{-1}{2}}, \quad \text{called the streaming Lorentz factor,} \qquad (32)$$

Solving these five simultaneous equations proved difficult for Mathematica. Numerical techniques failed to iterate to sufficiently accurate solutions. A graphical technique proved useful. It is straightforward to symbolically eliminate 3 of the 5 unknowns and arrive at two simultaneous equations. Plotting loci of solutions to these two equations, then finding any intersections enables one to find the remaining two unknowns and back-substitute to calculate the other three. Appendix E contains a copy of a Mathematica notebook used to perform this algorithm.

Unfortunately, the precision of this technique is limited. Mathematica will easily increase its precision for numerical calculations, but not for graphical plotting. This technique was unable to find any solutions with $\delta<10^{-16}$ or so. We will discover how much of a limitation this is in section 3.1.

$$N = 10^{38} s^{-1}, L = 10^{32} W, \Gamma = 10^5, \omega = 100 s^{-1}, \frac{\Omega_0}{\omega} = 1.76 \times 10^{11} \left(\frac{r}{r_L} \right)^{-2}$$

These are rough parameters, which were chosen for convenience.

$\frac{r}{r_L}$	δ	$\frac{\gamma^+}{\Gamma}$	$\frac{\gamma^-}{\Gamma}$	υ_0	ω_0 / s^{-1}
10^5	3.95 x 10^{-14}	1.049	1.048	1.06 x 10^6	0.015
10^6	2.927 x 10^{-11}	69.4	20.75	85000	0.0098
10^7	4.77 x 10^{-11}	114.4	5.69	7600	0.00033
10^8	4.98 x 10^{-11}	130	2.35	720	9.8 x 10^{-6}

The valid range of distance from the pulsar is from the light cylinder to the termination shock. This gives a range for $\frac{r}{r_L}$ of 1 to 10^9. Valid solutions could only be found for the range of $\frac{r}{r_L}$ shown above. Invalid solutions, with $\omega_0^2 < 0$ or $\frac{\gamma^{\pm}}{\Gamma} < 1$, were frequently found. Rough trends may be seen in the data, especially υ_0 and ω_0, but no real conclusions may be drawn from this incomplete set. Equation (11) gives us an upper limit on δ of $\frac{1}{2\Gamma^2}$ when $\Gamma >> 1$ and $\delta << 1$, and δ approaches this limit as $\frac{r}{r_L}$ increases.

3 - Analytic Solution to the Equations of Motion, with Approximations

Whilst I was toiling on Mathematica, my supervisor was having some analytic success, as detailed in appendix F.

He assumed:

$$\Gamma >> 1, \tag{33}$$

β very close to unity, (34)

$$\frac{\Omega_0}{\omega \gamma^{\pm} \left(1 - \frac{v_z^{\pm}}{\beta c} \right)} >> 1 \tag{35}$$

Equation (35), the *Strong Field Limit*, is satisfied for the pulsar at the centre of the Crab nebula at all distances from the pulsar in the range of interest. This is the most easily observed pulsar and is typically used as an example when one is required. In this limit, electrons and positrons obey identical equations of motion, cf (26) - (30). Now $\gamma^+ = \gamma^-$. We find that there are two distinct regions within the wind, which we call an Inner Wind and an Outer Wind. These are distinguished by the magnitude of *X*, where *X* is given by

$$X = \Gamma^2 \left(\frac{Ne^2}{8\pi\varepsilon_0 mc^3} \right)^{-1} \left(\frac{r}{r_L} \right)^2 \frac{\Omega_0^2}{\omega^2 \gamma} \tag{36}$$

Note that $X \propto r^{-2}$.

The Inner Wind region has $X >> 1$ and lies between $1 < \frac{r}{r_L} << 10^{6-7}$

The Outer Wind region has $X << 1$ and lies between $10^{6-7} << \frac{r}{r_L} < 10^{9}$

3.1 - Summary of Inner Wind Solution

$$\gamma^+ = \gamma^- = \Gamma \ , \tag{37}$$

$$\beta = 1 - \frac{Ne^2}{8\pi\varepsilon_0 mc^3}\frac{\omega^2}{4\Omega_0^2\Gamma^3}\left(\frac{r}{r_L}\right)^{-2} \tag{38}$$

$$\upsilon_0^2 = \frac{Ne^2}{8\pi\varepsilon_0 mc^3}2\left(\frac{L}{Nmc^2} - \Gamma\right)\left(\frac{r}{r_L}\right)^{-2} \tag{39}$$

The ratio of electromagnetic to kinetic energy in the Inner Wind can be calculated, and is constant.

$$L = 5\times10^{31}W, \Gamma = 4\times10^{6}, N = 1.5\times10^{38}s^{-1}, \omega = 190s^{-1}, \Omega_0 = 1.76\times10^{13}\left(\frac{\mathrm{r}}{\mathrm{r_L}}\right)^{-2} s^{-1}$$

These parameters are more realistic for the Crab pulsar.

$\frac{r}{r_L}$	$\log_{10}\delta$	ω_0 / s^{-1} (29)	υ_0	X	Strong Field Limit (35)
1	-27.51	889.8	9.59 x 10^{9}	0.503 x 10^{14}	0.75 x 10^{18}
10	-25.51	88.98	9.59 x 10^{8}	0.503 x 10^{12}	0.75 x 10^{16}
10^2	-23.51	8.898	9.59 x 10^{7}	0.503 x 10^{10}	0.75 x 10^{14}
10^3	-21.51	0.8898	9.59 x 10^{6}	0.503 x 10^{8}	0.75 x 10^{12}
10^4	-19.51	0.0889	9.59 x 10^{5}	0.503 x 10^{6}	0.75 x 10^{10}
10^5	-17.51	0.00898	9.59 x 10^{4}	0.503 x 10^{4}	0.75 x 10^{8}
10^6	-15.51	0.000885	9.59 x 10^{3}	50.3	0.75 x 10^{6}

These solutions were very accurate. I checked the accuracy by calculating both the left hand sides and right hand sides of (26) - (30). Only the $\frac{r}{r_L} = 10^6$ solution had errors greater than 0.1%. This had errors of up to a few percent, as expected from the size of *X*. Notice how the small size of δ prevented Mathematica from finding these solutions graphically.

3.2 - Summary of Outer Wind Solution

$$\gamma^+ = \gamma^- = \frac{L}{4Nmc^2}\left(1+\sqrt{1+8\left(\frac{L}{N\Gamma mc^2}\right)^{-2}}\right), \tag{40}$$

$$\delta = \frac{1}{2\Gamma^2}, \tag{41}$$

$$\upsilon_0^2 = \frac{Ne^2}{8\pi\varepsilon_0 mc^3}\left(\frac{r}{r_L}\right)^{-2}\frac{L}{Nmc^2}\left(\frac{3}{2}-\frac{1}{2}\sqrt{1+8\left(\frac{L}{N\Gamma mc^2}\right)^{-2}}\right), \tag{42}$$

The ratio of electromagnetic to kinetic energy in the Outer Wind can be calculated, and is constant.

$$L = 5\times10^{31}W, \Gamma = 4\times10^{6}, N = 1.5\times10^{38}s^{-1}, \omega = 190s^{-1}, \Omega_0 = 1.76\times10^{13}\left(\frac{r}{r_L}\right)^{-2}s^{-1}$$

$\frac{r}{r_L}$	$\log_{10}\delta$	$\frac{\gamma^{\pm}}{\Gamma}$	ω_0/s^{-1} (29)	υ_0	X	Strong Field Limit (35)
10^9	-13.5095	1.00547	8.900 x 10^{-8}	7.828	0.00005	75
10^8	-13.5509	1.00547	2.814 x 10^{-6}	78.279	0.005	750

These solutions were not as accurate as those in the Inner Wind region. The Outer Wind region is constrained on its inner boundary by the $X << 1$ requirement and on its outer boundary by the Strong Field Limit and the termination shock. In most of the small Outer Wind region, one of these is not very well satisfied. This accounts for the errors of a few percent in the above results.

When using Mathematica to graphically search for solutions (section 2.3), I did not find any solutions with these characteristics, though they should have been detectable with the parameters I was using. I believe that this is a consequence of the poor accuracy of approximations in this region. My Mathematica work would not have tolerated the errors of a few percent found here.

4 -Damping Times for Wave-like Pulsar Winds

To examine the stability of all these solutions against radiation loss, I evaluated the ratio of energy density in the wind and rate of loss of energy density in the wind. The energy density in the wind is calculated by summing the electromagnetic and kinetic contributions. The rate of loss of energy density in the wind is calculated using the relativistic generalisation of the Larmor formula for the power radiated by an isolated point charge. There is an implicit assumption here that the radiation fields of the charges do not interfere too much. The separation of the radiating charges must be greater than the characteristic wavelength of the emitted radiation. We have not yet checked this assumption, but hope it will not cause too drastic a correction.

As derived in appendix G, the damping time in cycles is given by

$$\omega\tau_d = \frac{6\pi\omega c^3\varepsilon_0 m}{e^2\omega_0^2}\frac{\left\{\frac{1}{2}\left(\frac{\Omega_0^2}{\omega}\right)\left(1-\left(1-\frac{1}{\Gamma^2}\right)^{\frac{1}{2}}\frac{1}{\beta}\right)+\frac{\upsilon_0^2}{2}\left(1+\frac{1}{\beta^2}\right)\left(1-\left(1-\frac{1}{\Gamma^2}\right)^{\frac{1}{2}}\frac{1}{\beta}\right)+\left(\frac{\omega_0}{\omega}\right)^2\left(\gamma^+ + \gamma^-\right)\right\}}{\left\{\gamma^{+2}\left(\frac{\gamma^{+2}}{\Gamma^2}-1\right)+\gamma^{-2}\left(\frac{\gamma^{-2}}{\Gamma^2}-1\right)\right\}} \tag{43}$$

As discussed in sections 1.2 and 1.3, we hope that the damping time will be greater than one cycle. For the solutions stated in sections 2.3, 3.1 and 3.2, I found the following damping times:

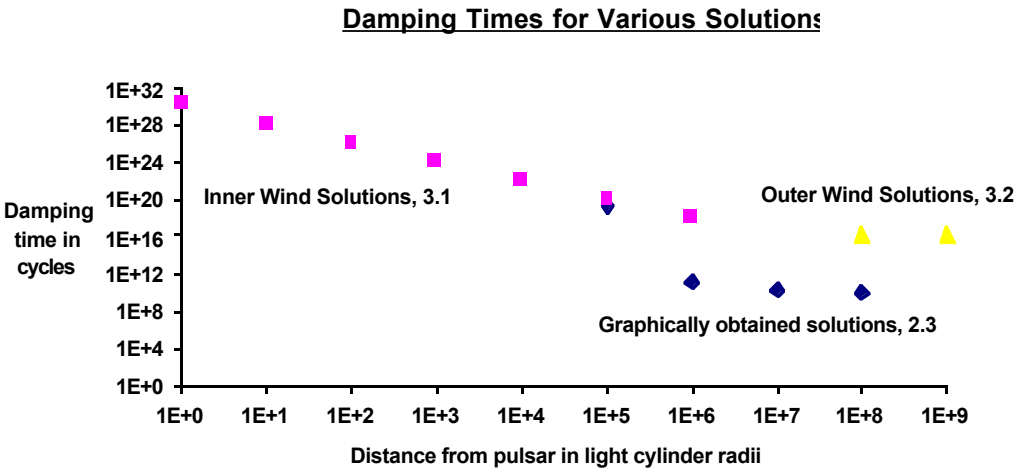

It is immediately apparent that all of these damping times are many orders of magnitude greater than a single cycle, and hence the wave-like model appears to be stable against radiative losses. It is straightforward to derive the inverse square behaviour of the Inner Wind's damping time and the constancy of the Outer Wind's damping time using the parameters given. Possibly the drastic change in the damping time observed for the graphically obtained solutions is indicative of a transition region in the wind. The difference between the graphically obtained mode and the Strong Field Limit mode(s) is again obvious. One might have expected (and we did) the damping times to increase as the wave moves away from the pulsar, as the intense fields weaken and the acceleration lessens. Equation (45) helps to explain the inverse square behaviour of the Inner Wind's damping time.

4.1 - Analytical Radiation Reaction Force

Reference to (2) - (3) gives one the impression that analytic work involving the Radiation Reaction is impossible, and we were unable to make any progress in that direction. My next approach was to use the undamped Inner Wind solution and "switch on the damping". In other words, evaluate the Radiation Reaction force for this solution and compare it with the Lorentz force. If the ratio is very much less than unity, then the undamped solutions will be valid and the stability will be confirmed. We concentrated on the Inner Wind because demonstrations of stability in this region will be most important to scientists working in the field, given the prevailing belief that damping times will increase away from the pulsar.

Appendix H derives the following result

$$\frac{\text{Lorentz force}}{\text{Radiation Reaction force}} = \frac{48\pi\varepsilon_0 mc^3\Gamma\Omega_0}{e^2\omega^2}\cot\chi \qquad (44)$$

$$= 2.536\times10^{39}\cot\chi \text{ , using the parameters given in section 3.1}$$

This result is for one of the transverse components of the force. The trigonometric factor is purely a consequence of quoting the result in this way, demonstrating that the particles are travelling along helical paths. This approach yields further insight. The change of variables required by (10) introduces

a factor of $\left(1-\frac{v_z}{\beta c}\right)^2$ into the Radiation Reaction force. This is very small indeed and reduces the radiated power. Also,

$$\frac{v_\perp}{c}=\frac{\upsilon_0\omega}{2\Gamma^2\Omega_0}\approx 3\times 10^{-15}\left(\frac{r}{r_L}\right). \qquad (45)$$

The constant streaming velocity (along the direction of propagation) is very large, yet the speed of rotation around the direction of propagation (and consequent acceleration) is very small. This makes the radiated power very small compared to the energy present, stabilising the wave. Why are the intense relativistic plasma waves in a pulsar wind so stable, unlike cases studied previously? The main new feature in this model is *streaming*, the transport of particles away from the pulsar. Both the effects described above would have no effect in the absence of streaming.

5 - Conclusion

There are major problems with the accepted steady-state model of pulsar winds, specifically the σ paradox and recent Hubble Space Telescope data. For a wave-like model to be accepted as an alternative, it must be stable. We have constructed an equilibrium solution for the wind as a wave, which conserves energy and particle number , and is extremely stable against radiation losses. The streaming of the wind away from the pulsar is crucial in stabilising the wave. Towards the end of my vacation project I began writing a Fortran program to integrate (1) - (7) numerically. This was extremely complicated algebraically and is presently in the debugging stages (all 35K of it). By choosing initial conditions corresponding to the undamped solution determined analytically in section 2.2 and then perturbing them slightly, we intend to verify the large radiative damping times found in section 4 and the analytic results of Bhatt under various hydromagnetic and radiative instabilities.

6-Acknowledgements

I am indebted to my supervisor, Andrew Melatos, for giving me the chance to spend summer in California. This work was funded by a Caltech Summer Undergraduate Research Fellowship (SURF) and NSF Grant AST-93-15455, with contributions from Queens' College, Cambridge and the Royal Astronomical Society, London.

References

Asseo, E., Kennel, C.F. & Pellat, R. 1978, *Astronomy & Astrophysics*, **65**, 401.

Hester, J. et al 1995, *Astrophysical Journal*, **448**, 240.

Kennel, C.F. & Coroniti, F. V. 1984, *Astrophysical Journal*, **283**, 694.

Max, C.E. and Perkins, F. 1972, *Physical Review Letters*, Volume 29, Number 26, 1730.

Melatos, A. and Melrose, D.B. 1996, *Monthly Notices of the Royal Astronomical Society*, **279**, 1168.

Shapiro, S.L. and Teukolsky, S.A. 1983, *Black Holes, White Dwarfs and Neutron Stars - The Physics of Compact Objects*, Wiley, New York.

Sweeney, G.S.S. and Stewart, P. 1978, *Astronomy and Astrophysics*, **66**, 139.

http://www.stsci.edu/pubinfo/PR/96/22.html

Graphically Obtained Solutions (Section 2.3)

$\frac{r}{r_L}$	$\omega\tau_d$
10^5	1.801×10^{19}
10^6	1.672×10^{11}
10^7	2.284×10^{10}
10^8	1.367×10^{10}

Inner Wind Region (Section 3.1)

$\frac{r}{r_L}$	$\omega\tau_d$
1	2.334×10^{30}
10	1.326×10^{28}
100	1.316×10^{26}
10^3	1.316×10^{24}
10^4	1.316×10^{22}
10^5	1.316×10^{20}
10^6	1.316×10^{18}

Outer Wind Region (Section 3.2)

$\frac{r}{r_L}$	$\omega\tau_d$
10^9	1.932×10^{16}
10^8	1.932×10^{16}